ORIGINAL ARTICLE

JBMR®

Bone Marrow Adiposity in Models of Radiation- and Aging-Related Bone Loss Is Dependent on Cellular Senescence

Abhishek Chandra,[1,2,3] Anthony B. Lagnado,[1,3] Joshua N. Farr,[1,3,4] Megan Schleusner,[3] David G. Monroe,[3,4] Dominik Saul,[3,4] João F. Passos,[1,2,3] Sundeep Khosla,[3,4] and Robert J. Pignolo[1,2,3,4]

[1]Department of Physiology and Biomedical Engineering, Mayo Clinic College of Medicine, Rochester, MN, USA
[2]Department of Medicine, Mayo Clinic College of Medicine, Rochester, MN, USA
[3]Robert and Arlene Kogod Center on Aging, Mayo Clinic College of Medicine, Rochester, MN, USA
[4]Division of Endocrinology, Mayo Clinic College of Medicine, Rochester, MN, USA

ABSTRACT

Oxidative stress-induced reactive oxygen species, DNA damage, apoptosis, and cellular senescence have been associated with reduced osteoprogenitors in a reciprocal fashion to bone marrow adipocyte tissue (BMAT); however, a direct (causal) link between cellular senescence and BMAT is still elusive. Accumulation of senescent cells occur in naturally aged and in focally radiated bone tissue, but despite amelioration of age- and radiation-associated bone loss after senescent cell clearance, molecular events that precede BMAT accrual are largely unknown. Here we show by RNA-Sequencing data that BMAT-related genes were the most upregulated gene subset in radiated bones of C57BL/6 mice. Using focal radiation as a model to understand age-associated changes in bone, we performed a longitudinal assessment of cellular senescence and BMAT. Using real-time quantitative reverse transcription polymerase chain reaction (qRT-PCR), RNA in situ hybridization of *p21* transcripts and histological assessment of telomere dysfunction as a marker of senescence, we observed an increase in senescent cell burden of bone cells from day 1 postradiation, without the presence of BMAT. BMAT was significantly elevated in radiated bones at day 7, confirming the qRT-PCR data in which most BMAT-related genes were elevated by day 7, and the trend continued until day 42 postradiation. Similarly, elevation in BMAT-related genes was observed in bones of aged mice. The senolytic cocktail of Dasatinib (D) plus Quercetin (Q) (ie, D + Q), which clears senescent cells, reduced BMAT in aged and radiated bones. MicroRNAs (miRNAs or miRs) linked with senescence marker *p21* were downregulated in radiated and aged bones, whereas miR-27a, a miR that is associated with increased BMAT, was elevated both in radiated and aged bones. D + Q downregulated miR-27a in radiated bones at 42 days postradiation. Overall, our study provides evidence that BMAT occurrence in oxidatively stressed bone environments, such as radiation and aging, is induced following a common pathway and is dependent on the presence of senescent cells. © 2022 American Society for Bone and Mineral Research (ASBMR).

KEY WORDS: AGING; BONE MARROW ADIPOSITY; CELLULAR SENESCENCE; P21; RADIATION

Introduction

Mechanisms underlying bone deterioration during physiological and pathological conditions have been a focus of study for many years. The balance between bone-forming osteoblasts and bone-resorbing osteoclasts maintains normal bone coupling, and marked deviation from this well-orchestrated mechanism causes either osteoporosis (due to comparatively more osteoclast function) or osteopetrosis (due to relatively increased bone formation with no or minimal bone resorption).[1] In common physiological conditions, such as aging or postmenopausal status, osteoporosis is the more prevalent condition and also associated with increased marrow fat or bone marrow adipose tissue (BMAT).[2] BMAT in humans has been shown throughout the lifespan with no potential side effects on bone architecture up to a certain age; but with aging, disease, and postmenopausal status, the presence of marrow fat appears to be inversely proportional to bone mass.[3] BMAT has also been used as a predictor of bone loss, showing a direct correlation to osteoporosis.[4]

An increase in BMAT has been associated with depleted resident mesenchymal stem cells (MSCs) during aging and disease, because MSCs are a common precursor to both adipocytes and

Received in original form December 10, 2021; revised form February 22, 2022; accepted February 27, 2022.
Address correspondence to: Abhishek Chandra and Robert J. Pignolo, Department of Physiology and Biomedical Engineering, Mayo Clinic College of Medicine, Rochester, MN, USA. E-mail: chandra.abhishek1@mayo.edu and pignolo.robert@mayo.edu
Additional Supporting Information may be found in the online version of this article.
Journal of Bone and Mineral Research, Vol. 37, No. 5, May 2022, pp 997–1011.
DOI: 10.1002/jbmr.4537

osteoblasts. In fact, with aging, MSCs undergo linage switching toward an adipogenic fate.[5-7] Only recently is it better understood that marrow fat cells have an autocrine, paracrine, and endocrine function, with local and systemic effects.[8] In observations made by multiple studies, bone resorption and BMAT are directly related, but adipocyte-secreted factors that regulate bone resorption or those that potentially affect bone formation are still unknown.

Cellular senescence is a nonproliferative, biologically active state[9] that produces an active secretome known as the senescence-associated secretory phenotype (SASP).[10] Cellular senescence is one of the key underlying mechanisms accounting for age- and radiation-related bone deterioration.[11-13] In bone tissue, senescence and SASP have been reported in osteoblasts, osteocytes, osteoprogenitors, and myeloid cells, with senescent myeloid cells and osteocytes being the major contributors to the SASP.[12] We have shown that BMAT is correlated with the presence of DNA damage, and mitigation of DNA damage can reduce BMAT and improve bone architecture postradiation.[5,14] We have also shown that focal radiation emulates several age-associated phenotypes[15] with an increase in markers of senescence and SASP in bone marrow cells, osteoblasts, and osteocytes.[11] Interestingly, we have shown that *p21* expression was more robust at earlier time points postradiation than $p16^{Ink4a}$, whereas $p16^{Ink4a}$ peaked much later.[11] We have previously observed a reduction in BMAT following clearance of senescent cells in aged and radiated bones.[11,13] However, a comprehensive molecular comparison between radiation-induced BMAT and aging-induced BMAT has not yet been described.

The spectrum of adipokines that increase with cellular senescence and have the potential to cause detrimental systemic effects are still unknown. To understand the triggers for accumulation of BMAT during aging and potential adipokine-associated genes, we used a radiation model to perform a longitudinal gene expression analysis of BMAT-related genes in young mice and compared them with those of bone tissue from old mice. We also explored the sequence of events early after radiation, to understand whether senescence precedes the accumulation of BMAT. Finally, we describe the relationships among BMAT, microRNAs (miRNAs or miRs) that regulate adiposity, and cellular senescence in *in vivo* models of focal radiation to bone, age-related bone loss, and pharmacologic clearance of senescent cells.

Materials and Methods

Animal study design

All animal studies were approved by the Institutional Animal Care and Use Committee at the Mayo Clinic. The animals were purchased from The Jackson Laboratory (Bar Harbor, ME, USA) and housed in our facility at 23°C–25°C with a 12-hour light/dark cycle and were fed with standard laboratory pellets with free access to water. Four-month-old C57BL/6 male mice received focal radiation as a single dose of 24 Gy on day 0. Because C57BL/6 female mice have very little bone mass postmaturity, we have used male mice in all our previously published studies involving radiation as an inducer of osteoporosis. Using X-Rad-SmART (Precision X-Ray (PXi), North Branford, CT, USA) an image-guided focal dose of 24 Gy at 6.6 Gy/min was delivered to a 5-mm region of the distal metaphyseal region of the right femur, while the left femur served as the contralateral control. The use of a 5-mm collimator provides submillimeter accuracy with the help of an image-guided system that ensures the radiation dose is limited to the region of interest and does not deliver any radiation outside this 5-mm region. Quality control is confirmed by regular dosimetry checks by the Department of Radiation Oncology at Mayo Clinic, which not only maintains the X-Rad-smART system, but also ensures precision delivery of the dose. SmART Plan software with state-of-the-art Monte Carlo algorithms enables researchers to accurately plan, visualize, and ultimately optimize treatment dose prior to therapy. We have shown that this method does not cause any abscopal side effects in the contralateral non-radiated bones.[5,11] This regimen is used with patients suffering from spinal metastases and is used as a proof of concept and an attempt to mimic patients with oligometastatic cancers to spine (mostly prostate and lung primary), treated with stereotactic body radiation therapy (SBRT) at our institution. SBRT with 24 Gy given as single dose[16,17] or two daily fractions[18] is increasingly used to treat spinal metastases, especially in oligometastatic patients, but it is accompanied by the risk of vertebral body fractures, especially in older individuals.[19-21]

Bones were harvested at days 1, 7, 21, and 42 for gene expression and RNA sequencing (day 21). Additional animals were radiated, and bones were collected on days 1 and 7 for histology and RNA in situ hybridization (RNA-ISH). Additionally, whole tibias were used to collect mRNA from 5-month-old and 24-month-old C57BL/6 mice ($n = 5$/ group) for comparison between young and aged bones. To test the effect of senolytic cocktail Dasatinib (D, 5 mg/kg) and Quercetin (Q, 50 mg/kg) on radiation-induced BMAT-related genes, D + Q was dosed on day 0 and day 14 post-radiation as described, and bones were collected on day 42 post-radiation.[11] To test the effect of D + Q on age-related BMAT, 20-month-old C57BL/6 mice were injected with vehicle or D + Q once monthly for 4 months as described,[13] with assessments of BMAT performed in the vertebra. For all experiments, the animals were given a unique code and the studies were performed in a double-blinded manner. None of the animals faced any adverse events or complications due to radiation.

RNA preparation, sequencing, and bioinformatics

A 5-mm region below the growth plate of the distal metaphyseal femur was cut out from the radiated (R) and non-radiated (NR) legs. After removal of muscle tissue, the bone samples, which may include surface-adherent osteoblasts or bone lining cells, vessel adhering pericytes, mesenchymal progenitors, osteocytes, and bone marrow cells, were homogenized and total RNA was isolated using RNeasy Mini Columns (QIAGEN, Valencia, CA, USA) for subsequent RNA-sequencing, which was performed by the Mayo Sequencing Core. MAP-RSeq version 3.0.2,[16] an integrated RNA-Seq bioinformatics pipeline developed at the Mayo Clinic, was used for comprehensive analysis of raw RNA sequencing paired-end reads. MAP-RSeq employed STAR (build mm10),[17] the very fast, accurate, and splice-aware aligner for aligning reads to the reference mouse genome. The aligned reads were then processed through multiple modules in a parallel fashion. Gene and exon expression quantification was performed using the Subread[18] package to obtain both raw and normalized (fragments per kilobase of transcript per million mapped reads [FPKM]). STAR-Fusion, a module to detect fusions in STAR,[17] was used to identify and report any expressed gene fusions in the samples. Likewise, expressed single nucleotide variants (SNVs) and small insertions-deletions (INDELs) were detected using a combination of bioinformatics tools such as GATK,[19] HaplotypeCaller,[19] and RVBoost.[20] Finally, comprehensive quality control modules from the

RSeQC[21] package were run on the aligned reads to assess the quality of the sequenced libraries. Results from these modules were linked through a single html document and reported by MAP-RSeq.

R bioinformatics package DESeq2 (1.32.0)[22] was used for differential gene expression analysis. The criteria for selection of significant differentially expressed genes were Benjamini-Hochberg–adjusted p value ≤0.05 and $|\log_2$ fold change$|$ ≥1.5. Subsequently, the EnhancedVolcano package (1.8.0) was used for visualization. For the heat map, a Z-score was calculated, and adipogenic genes depicted according to decreasing $\log_2$ fold change. The RNA-Seq data has been uploaded on the Gene Expression Omnibus (GEO) database (https://www.ncbi.nlm.nih.gov/geo/query/acc.cgi?acc=GSE180076).

Adipocyte differentiation assay

Human MSCs were maintained in growth media (Dulbecco's Modified Eagle Medium [DMEM; Gibco, Grand Island, NY, USA] containing D-glucose [1 g/L], L-Glutamine, and sodium pyruvate [110 mg/L]) supplemented with 10% fetal bovine serum (Gibco). For adipocyte differentiation, cells were cultured in growth media supplemented with indomethacin (60μM), isobutyl methylxanthine (500μM), dexamethasone (1μM), and insulin (10 μg/mL). Cells were cultured in growth media or adipocyte differentiation media for 14 days. Adipocyte differentiation was confirmed by visually confirming the lipid droplet accumulation by oil red staining (Fig. S2A). From a parallel culture mRNA was collected from control ($n = 2$) and adipogenic differentiated cells ($n = 2$) for gene expression analysis.

Telomere fluorescence in situ hybridization (FISH) and DNA damage

Paraffin embedded bone sections were deparaffinized followed by serial hydration in 100% and 70% ethanol, with final hydration in PBS. Antigen was retrieved by incubation in 0.01M citrate buffer (pH 6.0) at 95°C for 15 minutes, placed on ice for 15 minutes, and then washed in water and PBS for 5 minutes each. Subsequently, blocking buffer was applied (normal goat serum 1:60 in PBS/bovine serum albumin [BSA]; Vector Laboratories, Burlingame, CA, USA; #S-1000) for 30 minutes at room temperature (RT) followed by primary antibody (γ-H2A.X; Cell Signaling Technology, Danvers, MA, USA; mAb #9718) overnight at 4°C. Slides were washed three times with PBS and incubated for 60 minutes with a species-specific secondary antibody (Vector Laboratories; no. PK-6101). Sections were then washed three times in PBS for 5 minutes and Cy5 Streptavidin (1:500 in PBS; Vector Laboratories; no: SA-1500) was applied for 25 minutes followed by three washes in PBS, crosslinking with 4% paraformaldehyde for 20 minutes and dehydration in graded ethanol. Sections were denatured for 10 minutes at 80°C in hybridization buffer (70% formamide [Millipore Sigma, Gillingham, UK], 25mM $MgCl_2$, 0.1M Tris [pH 7.2], 5% blocking reagent [Roche Diagnostics, Mannheim, Germany]) containing 2.5 μg/mlCy-3-labeled telomere-specific (CCCTAA) peptide nucleic acid probe (Panagene, Daejeon, South Korea), followed by hybridization for 2 hours at RT (minimum) in a humidified chamber in the dark. Next, slides were washed once with 70% formamide in 2 × saline sodium citrate (SSC) for 10 minutes, followed by one wash in SSC and PBS for 10 minutes. Sections were mounted with Dapi (ProLong™ Diamond Antifade Mountant; Invitrogen, Carlsbad, CA, USA; P36962). In-depth Z-stacking was used (a minimum of 135 optical slices using a 63× objective). Number of telomere dysfunction–induced foci (TIFs) per cell was assessed by manual quantification of partially or fully overlapping (in the same optical slice, Z) signals from the telomere probe and γH2A.X in z-by-z analysis. Images were deconvolved with blind deconvolution in AutoQuant X3 (Media Cybernetics, Rockville, MD, USA).

For formalin-fixed paraffin-embedded (FFPE) tissue, immunohistochemistry was carried out following an overnight incubation with rabbit monoclonal anti-perlipin1 (1:100; Cell Signaling Technology; 9349). The next day following three washes, tissues were incubated with a species-specific secondary antibody (Alexa 647) for 1 hour then washed three times with PBS and mounted using ProLong Gold Antifade Mountant with 4′,6-diamidino-2-phenylindole (DAPI) (Invitrogen).

RNA-ISH and immunohistochemistry

RNA-ISH was performed on FFPE tissues per the RNAScope protocol (RNAScope Multiplex Fluorescent Assay v2) from Advanced Cell Diagnostics (Newark, CA, USA). Briefly, the assay allows simultaneous visualization of up to four RNA targets, with each probe assigned a different channel (C1, C2, C3, or C4). Each channel requires its own amplification steps; eg, p21 (CDKN1A) C1 probe was amplified by HRP-C1, followed by the addition of whichever fluorophore was assigned to that probe/channel using the Opal dyes (Opal 570 [Cy 3 Range]), then blocked to perform the next amplification in another channel, p16/p19 (CDKN2A) C3 using Opal 650 (Cy5). Tissue sections were then mounted using ProLong Gold Antifade Mountant with DAPI (Invitrogen). Sections were imaged using in-depth Z stacking.

Real-time quantitative reverse transcription polymerase chain reaction

A 5-mm region below the growth plate of the distal metaphyseal femur was cut out from the radiated and the non-radiated legs. After removal of muscle tissue, the bone samples were stored in TRIzol (Invitrogen) at −80°C. Bones were homogenized and total RNA was isolated using a phase separation method, followed by a RNase-free DNase treatment to remove genomic DNA and a cleanup of samples with the RNeasy Mini Columns (QIAGEN). The quality of the RNA was determined using a Nanodrop spectrophotometer with A260/230 ≥ 1.6 and A260/A280 set at ≥1.8 (Thermo Fisher Scientific, Waltham, MA, USA). The cDNA was generated from mRNA using the High-Capacity cDNA Reverse Transcription Kit (Applied Biosystems by Life Technologies, Foster City, CA, USA), according to the manufacturer's instructions.

Primers that were designed for our previous studies[12] were used for real-time quantitative reverse transcription polymerase chain reaction (qRT-PCR) in this study as well. Additional primers were designed using Primer Express® Software Version 3.0 (Applied Biosystems) (Table S1 and Table S2). Using a high throughput ABI Prism 7900HT Real Time System (Applied Biosystems, Carlsbad, CA, USA) with SYBR Green (QIAGEN) as the detection method, gene expression was detected. Gene expression was normalized against the average of two reference genes (Actb and Tuba1) and the fold difference between the reference gene and the target gene (reference threshold cycle [Ct] - gene of interest Ct) was calculated by comparing the median Ct with NR-femurs serving as control for R-femurs, and young bone cells serving as controls for old.

Table 1. List of Genes Related to Adipocyte Function Characterized as Secretory or Nonsecretory Proteins Based on a Signal Sequence Predictor Bioinformatic Tool, Signal P 5.0

Gene name	Description	Secretory protein prediction (using signal P 5.0)[a]	Cell type (reference)
Adipoq	Adiponectin	Yes	Human-adipose derived stem cells (ASC)[42]
Cidec	Cell death-inducing DFFA-like effector c	No	
Plin1	Perilipin 1	No	
Gpd1	Glycerol-3-phosphate dehydrogenase 1	No	
Mlxipl	MLX interacting protein-like	No	
Igf1	Insulin like growth factor 1	No	
Pnpla3	Patatin-like phospholipase domain containing 3	No	
Tusc5/Trarg1	Trafficking regulator of GLUT4 (SLC2A4) 1	No	
Aoc3	Amine oxidase, copper containing 3	No	
Lipe	Lipase E, hormone sensitive type	No	
Mcam	Cell surface glycoprotein MUC18	Yes	
Glul	Glutamate-ammonia ligase	No	
Pde3b	Phosphodiesterase 3B	No	
Fabp4	Fatty Acid Binding Protein 4	No	ASC,[42] Microarray[43] [44]
Cxcl13	Chemokine (C-X-C motif) ligand 13	Yes	
Plin4	Perilipin 4	No	ASC[42,45]
Acvr1c	Activin A receptor, type IC	Yes	3T3L1, SVF cells[46] Human BM-MSC[47]
Cfd	Complement factor D/Adipsin	Yes	ASC,[42] 3T3L1, WAT[43] Human BM-MSC[47]
Pparg	Peroxisome Proliferator Activated Receptor Gamma	No	
Atp1a2	ATPase, Na+/K+ transporting, alpha 2	No	SW872[48]
Thrsp	Thyroid hormone responsive	No	Human adipocytes[49]
Lgals12	Galectin 12	No	3T3L1, human adipose tissue[50]
Igf2	Insulin-like growth factor 2	Yes	Rat ADSC[51]
Rbp4	Retinol binding protein 4	Yes	Human multipotent adipose tissue-derived stem cells (hMADS)[52]
Fabp5	Fatty acid binding protein 5	No	
Nr1h3	Oxysterols Receptor LXR-Alpha	No	
Lpl	Lipoprotein lipase	Yes	3T3L1, White adipose tissue (WAT)[43]
Scd1	Stearoyl-CoA desaturase 1	No	
Lep	Leptin	Yes	
Rarres2	Retinoic acid receptor responder (tazarotene induced) 2, Chemerin	Yes	3T3L1[53]
Ccdc3	Coiled-coil domain containing 3	Yes	Rat primary adipocytes and adipose tissue[54]
Col5a3	Collagen type V alpha 3 chain	Yes	Human BM-MSC[47]
Igfbp5	Insulin like growth factor binding protein 5	Yes	
Plin2	Perilipin 2	No	
Ghr	Growth hormone receptor	Yes	
Rxra	Retinoid X Receptor Alpha	No	
Agpat9	Glycerol-3-phosphate acyltransferase 3	No	3T3L1[55] [56]
Igfbp7	Insulin-like growth factor binding protein 7	Yes	
Ctsc	Cathepsin C/ Dipeptidyl peptidase 1	Yes	
Plin2	Perilipin 2	No	Adipose tissue[57]
Alcam	CD166 antigen	Yes	
Ankef1	Ankyrin repeat and EF-hand domain-containing protein 1	No	

[a]"Yes" stands for secretory and "No" stands for nonsecretory.

Statistical analysis

The sample size for each experiment was determined based on prior experience and available data sets. Individual animals were treated as indicated in the figure legends. The R-based tool from Bioconductor, edgeR (3.32.1), was used to perform the differential expression analysis. Those mature mRNAs were significantly differentially expressed at a p value <0.05 and a $\log_2$ fold change >1 or < −1. Heat maps were created using GraphPad Prism 9.3.1. (GraphPad Software, Inc., La Jolla, CA, USA).

For the Search Tool for the Retrieval of Interacting Genes/Proteins (STRING) protein analysis, the 56 differentially expressed genes indicated in Table 1 were selected, and a full evidence-based network was created (high confidence 0.7[23]). The node degrees were exported to Cytoscape (3.8.2; https://cytoscape.org/) and a functional STRING enrichment retrieved. Likewise,

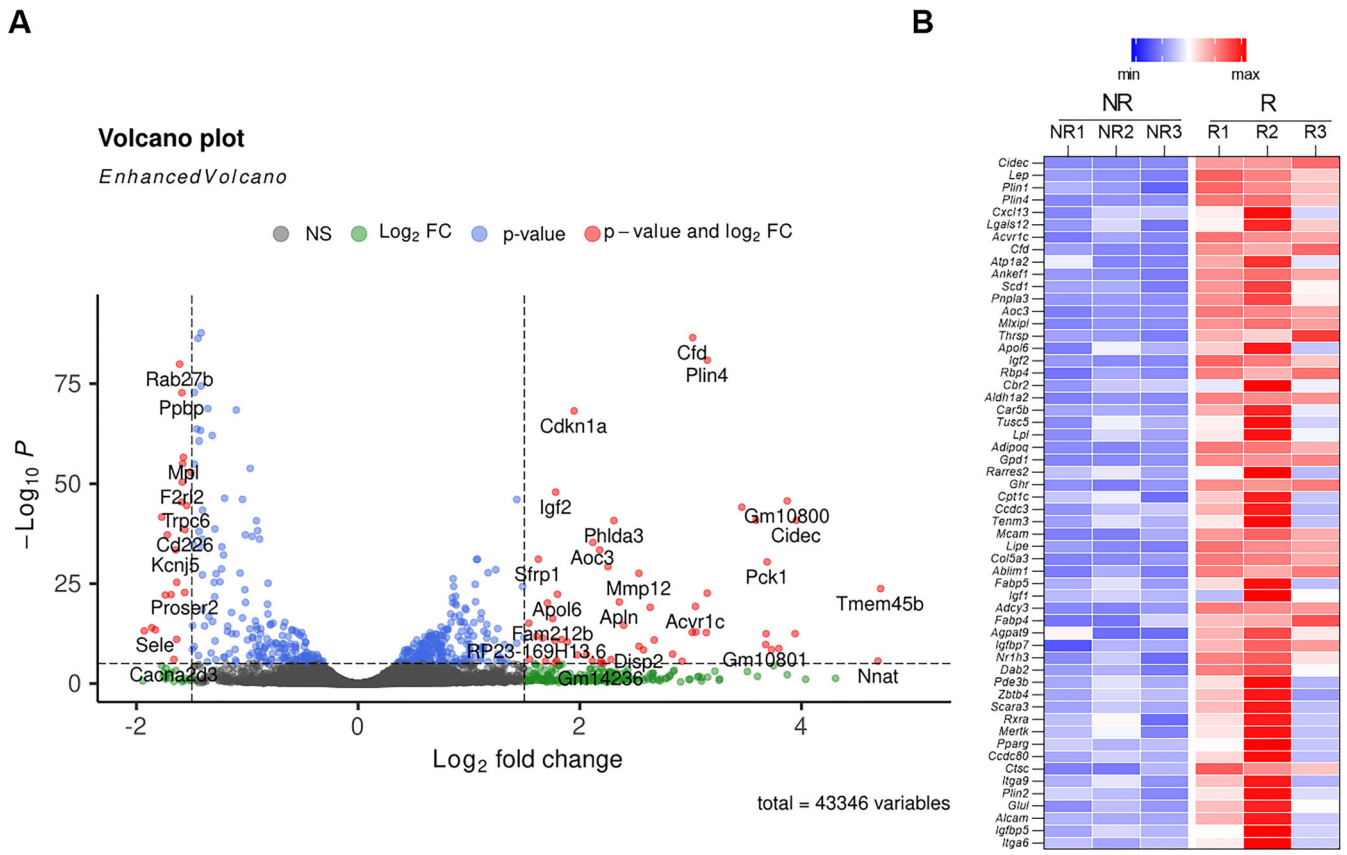

Fig. 1. Volcano plot of the transcriptome in the radiated bones. (*A*) The right femoral metaphyses of C57BL/6 mice ($n = 3$) were radiated (24 Gy) in a 5-mm region, while the equivalent region of the left leg served as control. R and NR femurs at day 21 postradiation were harvested for mRNA isolation. Volcano plots were generated to present the RNA-Seq data. Volcano plots of differentially expressed genes were generated based on Benjamini-Hochberg adjusted *p* values after DESeq2 analysis (1.32.0). The horizontal line and vertical lines indicate the significance threshold ($|p_{adj}| < 0.05$) and twofold change threshold ($|\log_2\text{FoldChange}| > 1.5$), respectively. The DEGs are shown with red dots while non-DEGs are in black. Upregulated DEGs with a $\log_2$Fold Change of ≥1.5 (but $p_{adj} < 0.05$) in the radiated bones are depicted with green-colored spots on the right side and downregulated DEGs with a $\log_2$Fold Change of ≥1.5 are depicted with green-colored spots on the left side. Blue dots indicate all significant changes without a $|\log_2\text{FoldChange}| > 1.5$. (*B*) A curated list of genes that are reported to be expressed during adipocyte cell differentiation was used to generate a heat map using their *Z*-scores of genes expressed in R and NR bones detected by RNA-Seq. They are arranged in descending order based on their $\log_2$FoldChange. DEG = differentially expressed gene.

the network was analyzed within Cytoscape as a directed graph, and the corresponding degree of interactions are depicted as sphere and label size. For D + Q studies, statistical analyses were done using GraphPad Prism and *p* values were calculated using a two-way ANOVA with a Tukey's post hoc test performed to compare vehicle-R with all the other groups. The D + Q studies done in the aging cohort were analyzed using a two-tailed unpaired *t* test. Statistical comparisons of young, old, and radiated miRs were done using one-way ANOVA with a Bonferroni post hoc test. A detailed statistical analysis for Figs. 4*B*,*D*,*F*, 6*C*, 7, and 8*C*, has been provided as Table S3.

Results

Gene expression of adipocyte-related genes in radiated bones

RNA isolated from a focally radiated 5-mm area of the femoral metaphysis 3 weeks postradiation was processed for RNA sequencing. Identified genes were then arranged based on their $-\log_{10}$ adjusted *p* value. The genes with the highest $\log_2$ fold change value when depicted using a volcano plot showed that the senescence marker *Cdkn1a* (*p21*) and several adiposity related genes (*Cidec*, *Plin1*, *Plin4*, *Lpl*, *Igf2*) were among the most upregulated genes, whereas genes that were associated with endothelial function (*Vwf*, *Ppbp*, *Pf4*, and *Mmrn1*) were among the most downregulated (Fig. 1*A*). Interestingly, at 3 weeks *Cdkn2a* ($p16^{Ink4a}$) was below detection levels. Fifty-six genes related to adipogenic differentiation in a variety of in vitro cell culture models were identified (Table 1) and a heat map was generated to see the expression pattern postradiation (Fig. 1*B*). The majority of these 56 select genes that may have a function during adipogenic differentiation were found to be upregulated in radiated bones.

A highly stringent STRING network suggested a subset of genes that were closely associated (Fig. S1A; average number of neighbors: 4.45; clustering coefficient 0.49; network density: 0.148) and were identified as genes part of the lipid metabolism

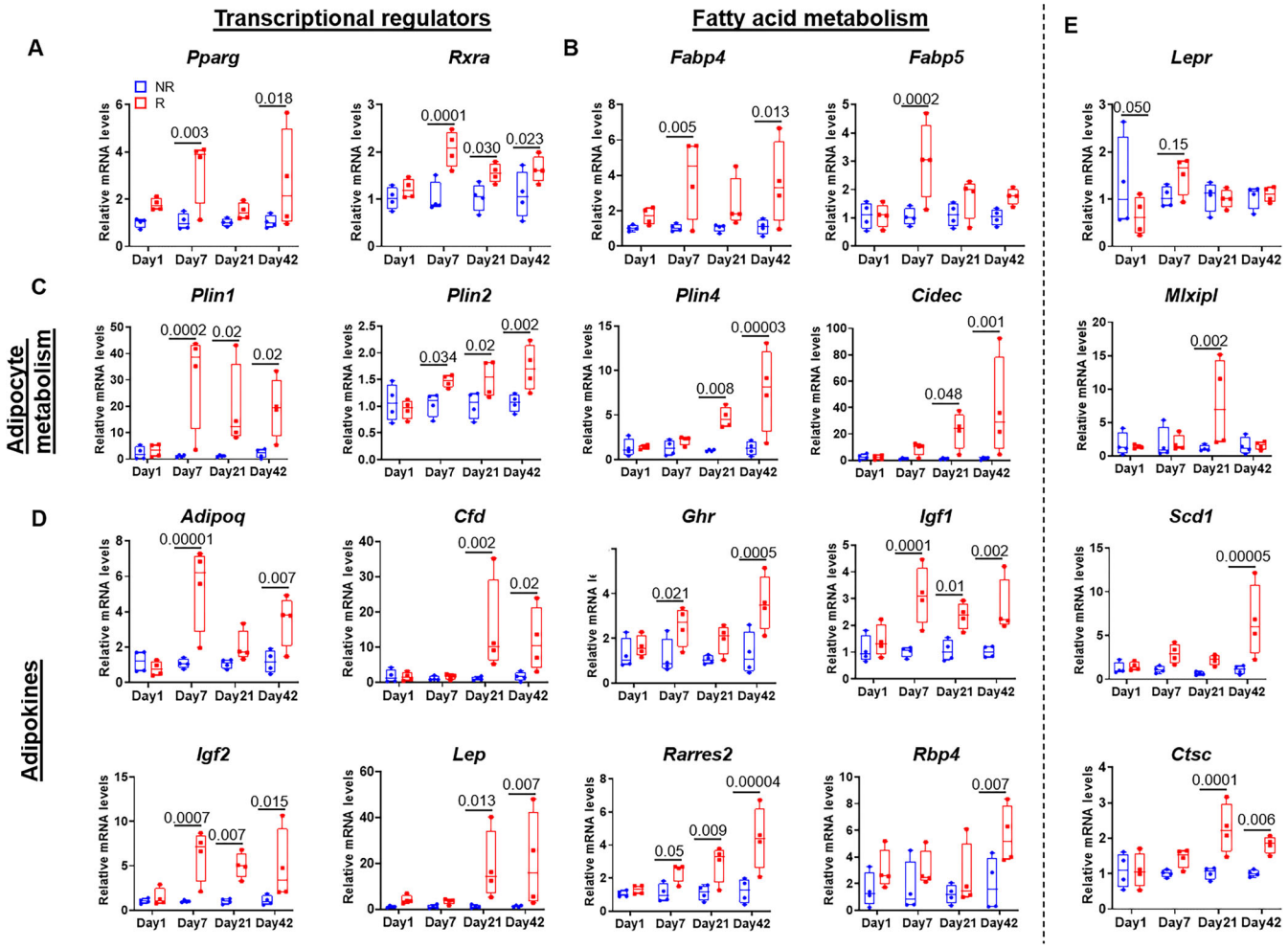

Fig. 2. Longitudinal assessment of adiposity-related genes in radiated bones. The right femoral metaphyses of C57BL/6 mice were radiated (24 Gy) in a 5-mm region, while the equivalent region of the left leg served as control. On days 1, 7, 21, and 42 ($n = 4$ for each time point) R and NR femurs were harvested for mRNA isolation. qRT-PCR analysis is shown for genes involved with (*A*) transcription regulation of adipogenesis, (*B*) fatty acid metabolism, (*C*) adipocyte metabolism, (*D*) adipokines, and (*E*) genes with miscellaneous functions during adipocyte differentiation. Data are shown as box-and-whisker plots (with median and interquartile range) from maximum to minimum, showing all data points. Statistical analyses were done using GraphPad Prism and *p* values were calculated using a two-tailed, paired *t* test.

pathways (Fig. S1B, lipid metabolic process false discovery rate [FDR] $= 8.15 \times 10^{-10}$). Using qRT-PCR, we confirmed the expression of these selected genes during adipocyte differentiation of human MSCs (Fig. S2).

Longitudinal assessment of adiposity-related genes in radiated mouse bone tissue

To confirm the longitudinal expression of BMAT-related genes postradiation, we analyzed 20 selected genes (as determined by the STRING network) on days 1, 7, 21, and 42 postradiation. We observed a nonsignificant elevation in the transcriptional regulators, *Pparg* and *Rxra*, on day1, followed by a sustained significant increase in both these genes on days 7, 21, and 42 (Fig. 2*A*). None of the other analyzed genes were significantly expressed on day 1 postradiation. Significant upregulation in adipose-associated genes related to metabolism and secretory adipokines was observed in R-bones at day 7 (*Adipoq*, *Fabp4*, *Fabp5*, *Ghr*, *Igf*-1, *Igf-2*, *Plin-1*, *Plin-2*, and *Rarres2*), day 21 (*Cfd*, *Ctsc*, *Igf-1*, *Igf-2*, *Lep*, *Mlxipl*, *Plin-1*, *Plin-2*, *Plin-4*, and *Rarres2*) and at day 42 (*Adipoq*, *Cfd*, *Cidec*, *Ctsc*, *Fabp4*, *Ghr*, *Igf-1*, *Igf-2*, *Lep*, *Plin-1*, *Plin-2*, *Plin-4*, *Rarres2*, *Rbp4*, and *Scd1*) (Fig. 2*B–E*). There were some genes that showed a nonsignificant elevation in R-bones at day 7 (*Cidec*, *Lepr*, and *Scd1*) and at day 21 (*Adipoq*, *Cidec*, *Fabp4*, *Ghr*, *Rbp4*, and *Scd1*).

Adiposity-related gene expression in old bone tissue

To understand the expression profile of BMAT-related genes during aging, we next performed qRT-PCR on 24-month-old bones. Eighteen genes related to adipocyte transcriptional regulation, metabolism, and secretory adipokines (*Adipoq*, *Cfd*, *Cidec*, *Ctsc*, *Fabp4*, *Ghr*, *Igf-1*, *Igf-2*, *Lep*, *Lepr*, *Mlxipl*, *Plin-1*, *Plin-2*, *Plin-4*, *Pparg*, *Rarres2*, *Rbp4*, and *Rxra)* (Fig. 3*A–D*) were significantly upregulated, as compared to young (5-month-old) mouse bone tissue. Unlike radiated bone, aged bone showed a sixfold increase in the leptin receptor (*Lepr*) (Fig. 3*E*).

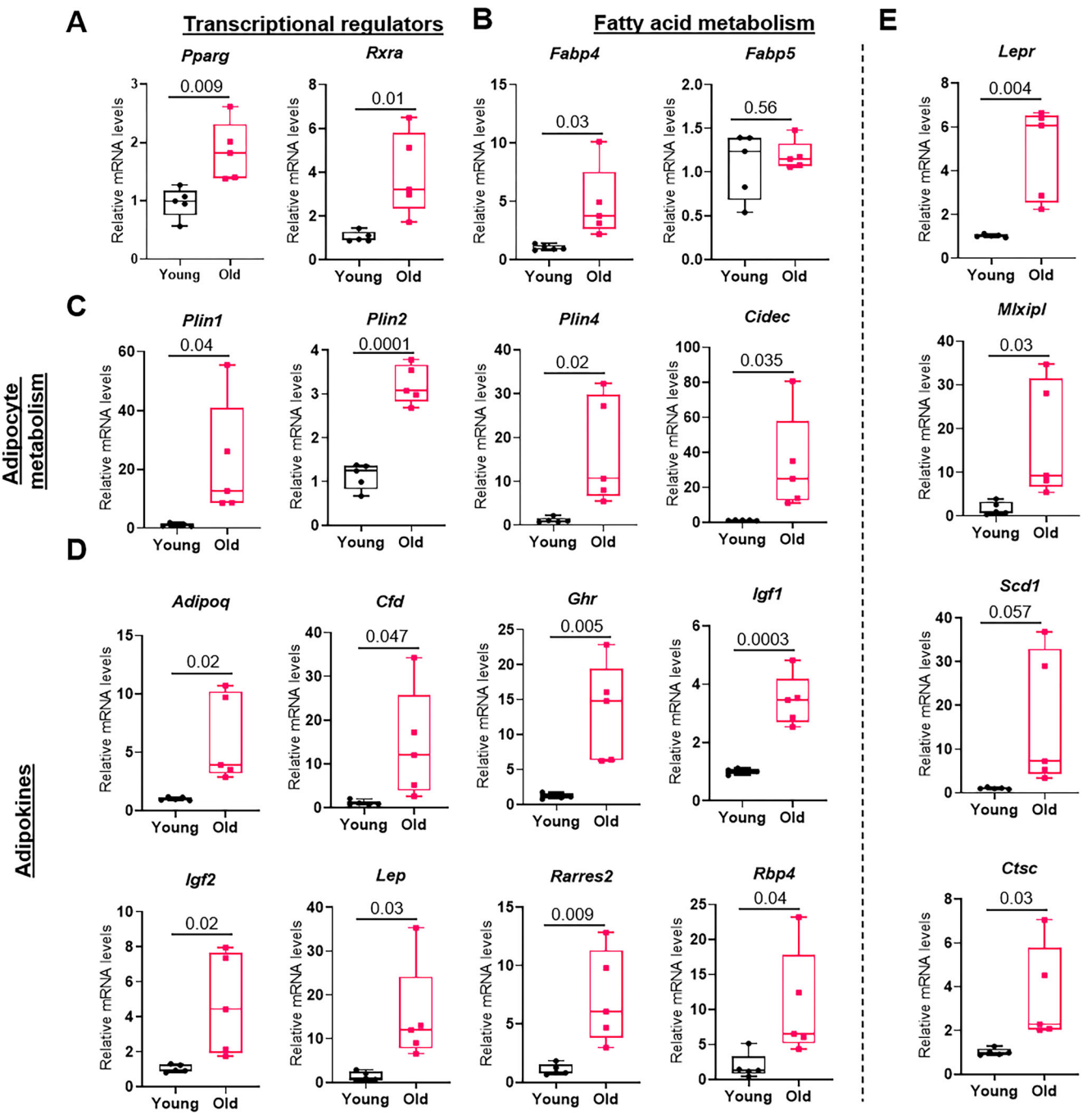

Fig. 3. Longitudinal assessment of adiposity related genes with aging. Whole bones were collected from young (5 months) ($n = 5$) and old (24 months) ($n = 5$) mice and mRNA were isolated. qRT-PCR analysis is shown for genes involved with (*A*) transcription regulation of adipogenesis, (*B*) fatty acid metabolism, (*C*) adipocyte metabolism, (*D*) adipokines, and (*E*) genes with miscellaneous functions during adipocyte differentiation. Data are shown as box-and-whisker plots (with median and interquartile range) from maximum to minimum, showing all data points. Statistical analyses were done using GraphPad Prism and *p* values were calculated using a two-tailed unpaired *t* test.

Assessment of senescence markers during aging and radiation

To understand the link between senescence and adiposity seen with radiation and aging, we first confirmed our previous report that high *p21* expression was seen at early time points postradiation, whereas $p16^{Ink4a}$ expression peaked at later time points (ie, day 42; Fig. S3A). Assessing gene expression in 24-month-old bone samples, we detected high *p21* (sixfold increase, $p = 0.0002$) and high $p16^{Ink4a}$ (3.5-fold increase, $p = 0.005$) gene expression as compared to 4-month-old young bone samples (Fig. S3B).

To further elucidate the dynamics of the cellular changes postradiation and to test whether senescence precedes BMAT expansion, we performed the TIF assay, which detects DNA damage at

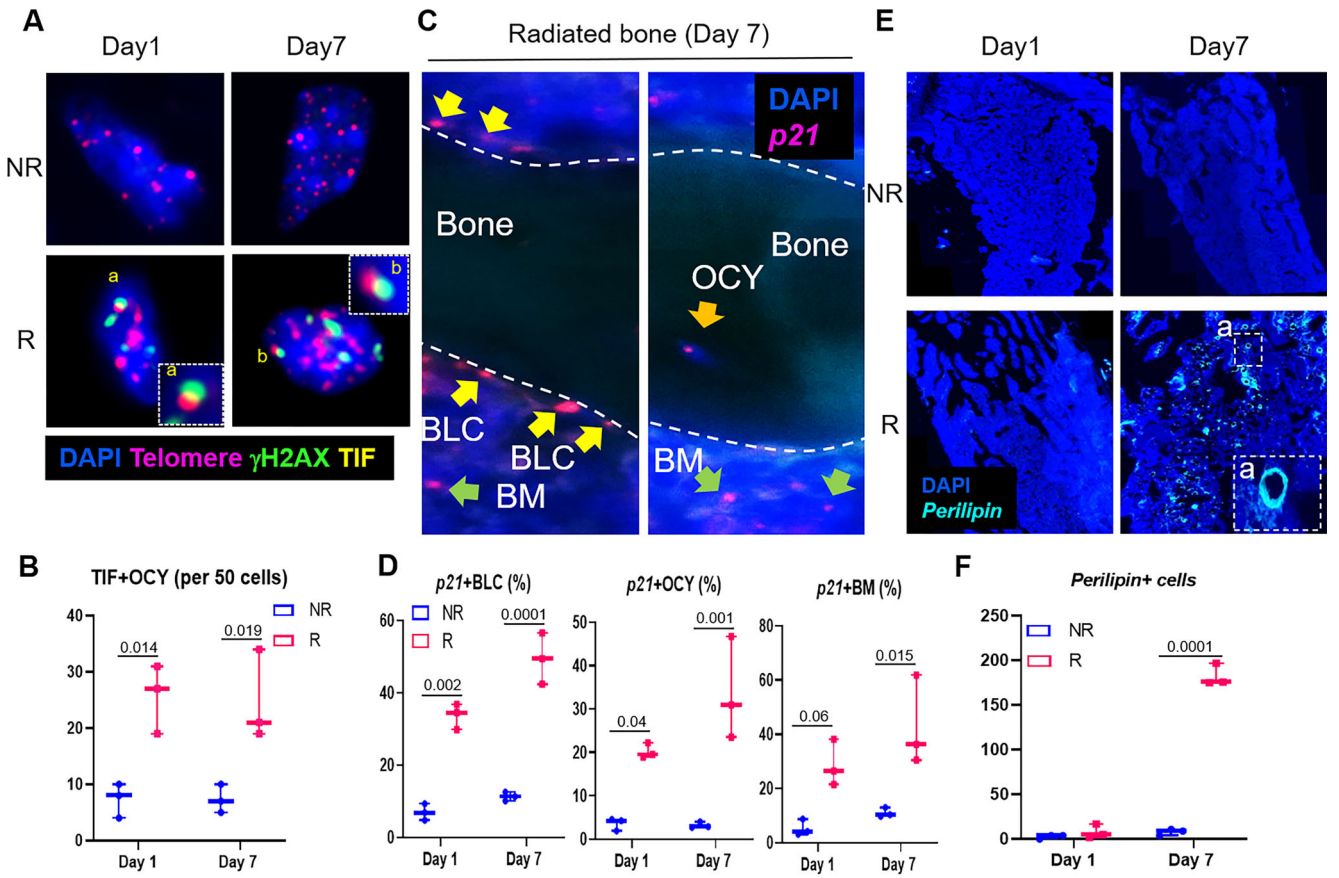

Fig. 4. Longitudinal assessment of senescent cells and adipocytes in radiated bone tissue. To elucidate the earliest occurrence of cellular senescence postradiation, R-bones and NR-bones were assessed for presence of senescent cells and adipocytes. (*A*,*B*) Colocalization of DNA damage at telomere sites, or TIF, was visualized (*A*) and TIF+ osteocytes were quantified (*B*) at days 1 and 7 postradiation. (*C*,*D*) RNA in-situ hybridization against *Cdkn1a* (*p21*) transcript was performed, visualized, and quantified in R-bones and NR-bones on days 1 and 7 and *p21*+ BLCs, OCYs, and BM cells. (*E*,*F*) Perilipin-stained adipocytes were assessed in NR-bones and R- bones. Negligible levels of adipocytes were identified in NR-bones, hence images are shown only for R-bones (*E*), whereas quantifications for both NR-bones and R-bones are presented (*F*). Data are shown as box-and-whisker plots (with median and interquartile range) from maximum to minimum, showing all data points. Statistical analyses were done using GraphPad Prism and *p* values were calculated using a two-way ANOVA ($\alpha = 0.05$) with a Tukey post hoc analysis. BLC = bone lining cell; BM = bone marrow; OCY = osteocyte; TIF = telomere dysfunction-induced foci.

telomeric sites (ie, dysfunctional telomeres), and observed significant upregulation in TIF$^+$ osteocytes on day 1 and day 7 (Fig. 4*A*,*B*). The detection of the *p21* transcript was performed using RNA-ISH, and *p21*$^+$-bone lining cells (BLCs), *p21*$^+$-osteocytes (OCY), and *p21*$^+$-bone marrow (BM) cells were detected on both days 1 and 7 postradiation (Fig. 4*C*,*D*). Perilipin staining confirmed that adipocytes were almost absent at day 1 postradiation, whereas substantial numbers of perilipin$^+$ adipocytes were observed at day 7 postradiation (Fig. 4*E*,*F*).

Changes in miRNAs that regulate p21

Based on their binding at the 3′-untranslated region (UTR) of *p21*, miRs were selected on their preferentially conserved targeting (PCT) as determined by the TargetScan tool, which predicts the biological targets of miRNAs by searching for conserved 8mer, 7mer, and 6mer sites that match the seed region of each miRNA (Fig. 5*A*). We selected *miR-106b-5p* and *mir-20a-5p*, two miRs that have also been shown to regulate *Cdkn1a* and human aging in general.[24,25] Significant downregulation of *mir-106b-5p* (targeting *p21* mRNA) was observed both in aged-bones ($p = 0.03$) and R-bones ($p = 0.04$), whereas *mir-20a-5p* showed a nonsignificant decrease in old bones, but a significant reduction in R-bones ($p = 0.009$) when compared to young-NR bone samples (Fig. 5*B*). The *mir-106b-5p* was substantially reduced at different time points in the radiated bone tissue (day 1 [$p = 0.045$], day 7 [$p = 0.02$], and day 21 [$p = 0.017$]), whereas *mir-20a-5p* was significantly downregulated only at day 21 postradiation ($p = 0.03$) but also had reduced expression throughout at day 1 and day 7 (Fig. 5*C*).

Suppression of senescent cell burden reduces BMAT and BMAT-associated genes

BMAT is a common observation following radiation exposure and aging. We have shown previously that intermittent treatment with the senolytic cocktail of D + Q can suppress

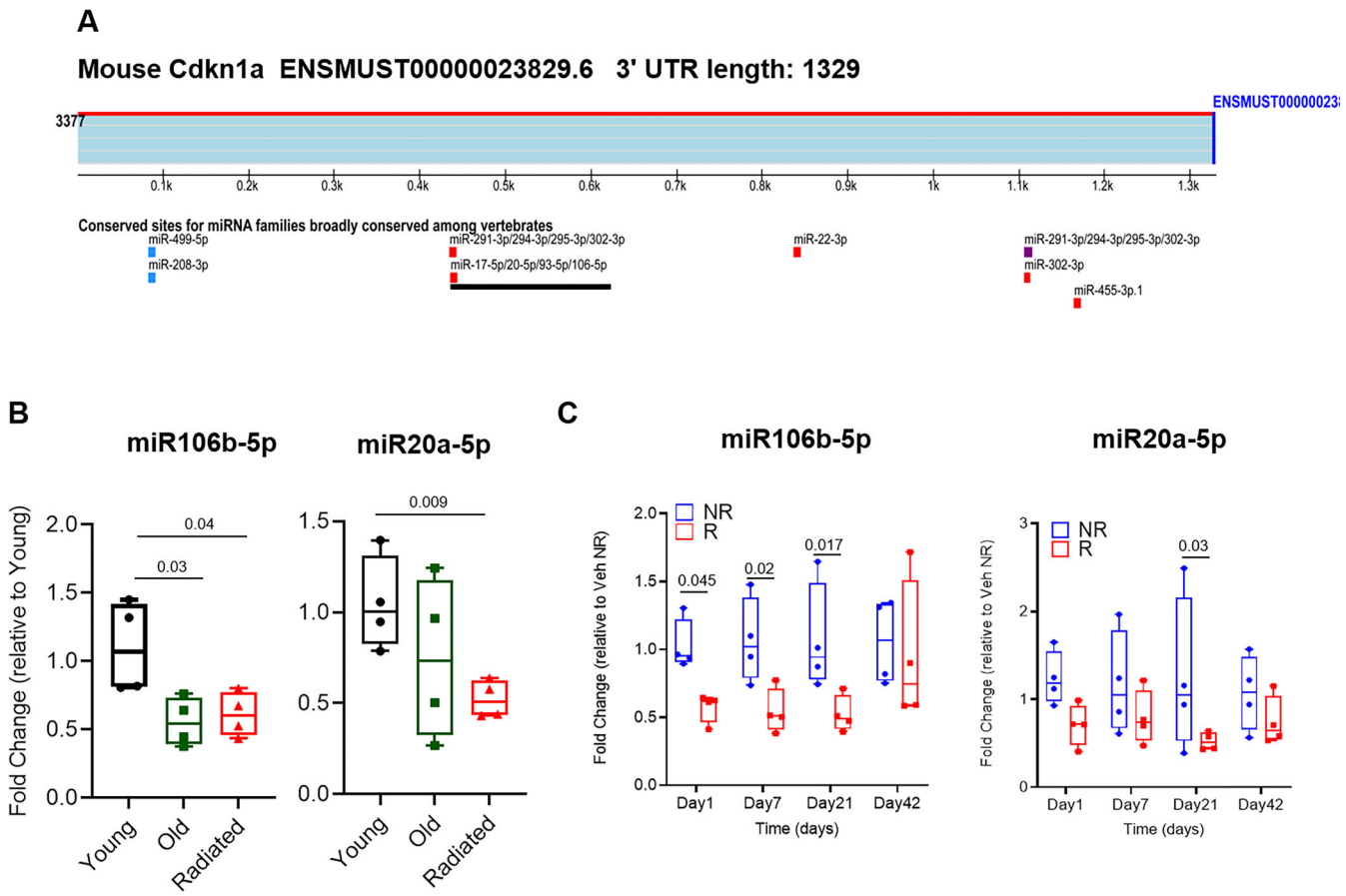

Fig. 5. microRNAs targeting *Cdkn1a* are downregulated in radiated and aged bones. (*A*) A schematic showing microRNAs that bind to the 3′ UTR of the senescence marker *Cdkn1a* (*p21*). (*B*) Whole bones were collected from young (5 months old, $n = 4$), old (24 months old, $n = 4$), and radiated (5 months old, $n = 4$) mice and mRNA were isolated. The cDNA was prepared using a miR reverse transcriptase kit and qRT-PCR was performed using the primers for miR-106b-5p and miR-20a-5p. Although miR-106b-5p was significantly reduced in both old bones and R-bones, miR-20a-5p showed a trend to decrease in old bones but reduced significantly in radiated bones. Statistical analyses were done using GraphPad Prism and *p* values were calculated using a one-way ANOVA ($\alpha = 0.05$) with a Bonferroni post hoc analysis. (*C*) To test the expression of miRs longitudinally, the right femoral metaphyses of C57BL/6 mice were radiated (24 Gy) in a 5-mm region, while the equivalent region of the left leg served as control. On days 1,7, 21, and 42 ($n = 4$ for each time point) R-femurs and NR-femurs were harvested for total mRNA isolation, cDNA was prepared using a miR reverse transcriptase kit, and qRT-PCR was performed using the primers for miR-106b-5p and miR-20a-5p. Significant reduction in the expression of miR-106b-5p was observed in R-femurs at days 1, 7, and 21. Although reduction was also observed in miR-20a-5p expression at all time points, significant changes were seen on day 21. Data are shown as box-and-whisker plots (with median and interquartile range) from maximum to minimum, showing all data points. Statistical analyses were done using GraphPad Prism and *p* values were calculated using multiple *t* tests.

senescent osteoblasts, osteocytes, and BM cells, and alleviate deleterious changes in bone architecture during aging[13] and post-focal radiation.[11] Assessments made for BMAT following intermittent treatment with D + Q following 24-Gy focal radiation (Fig. 6*A*) showed reduced BMAT, as measured by adipocyte number and volume, and normalized against the BM area (Fig. 6*B*,*C*). Similarly, intermittent treatment with D + Q (Fig. 6*D*) suppressed BM fat seen in aged bones (Fig. 6*E*), suggesting a direct role of the senescent microenvironment in promoting marrow adiposity. Furthermore, we found that BMAT-related genes were downregulated in radiated bones at day 42 postradiation following two doses of intermittent treatment with D + Q (Fig. 7), suggesting a direct role of a senescent cell burden on presence of BMAT.

Adipose-related *miR-27a-3p* is dependent on a senescence-driven microenvironment

Intriguingly, *mir-27a-3p*, reported to be elevated during obesity and in adipose tissue as a feedback for adipose-related transcription factor expression,[26] and shown to downregulate bone marker genes, was significantly elevated in aged-bones (25-fold increase, $p = 0.04$) and in R-bones (threefold increase, $p = 0.017$) (Fig. 8*A*). Upregulation of *mir-27a-3p* was also observed in R-bones at different time points (day 1 [$p = 0.004$], day 21 [$p = 0.17$], and day 42 [$p = 0.031$] (Fig. 8*B*). Treatment with the senolytic cocktail of D + Q suppressed the upregulation seen in *mir-27a-3p* levels in bones at 4 weeks postradiation (Fig. 8*C*).

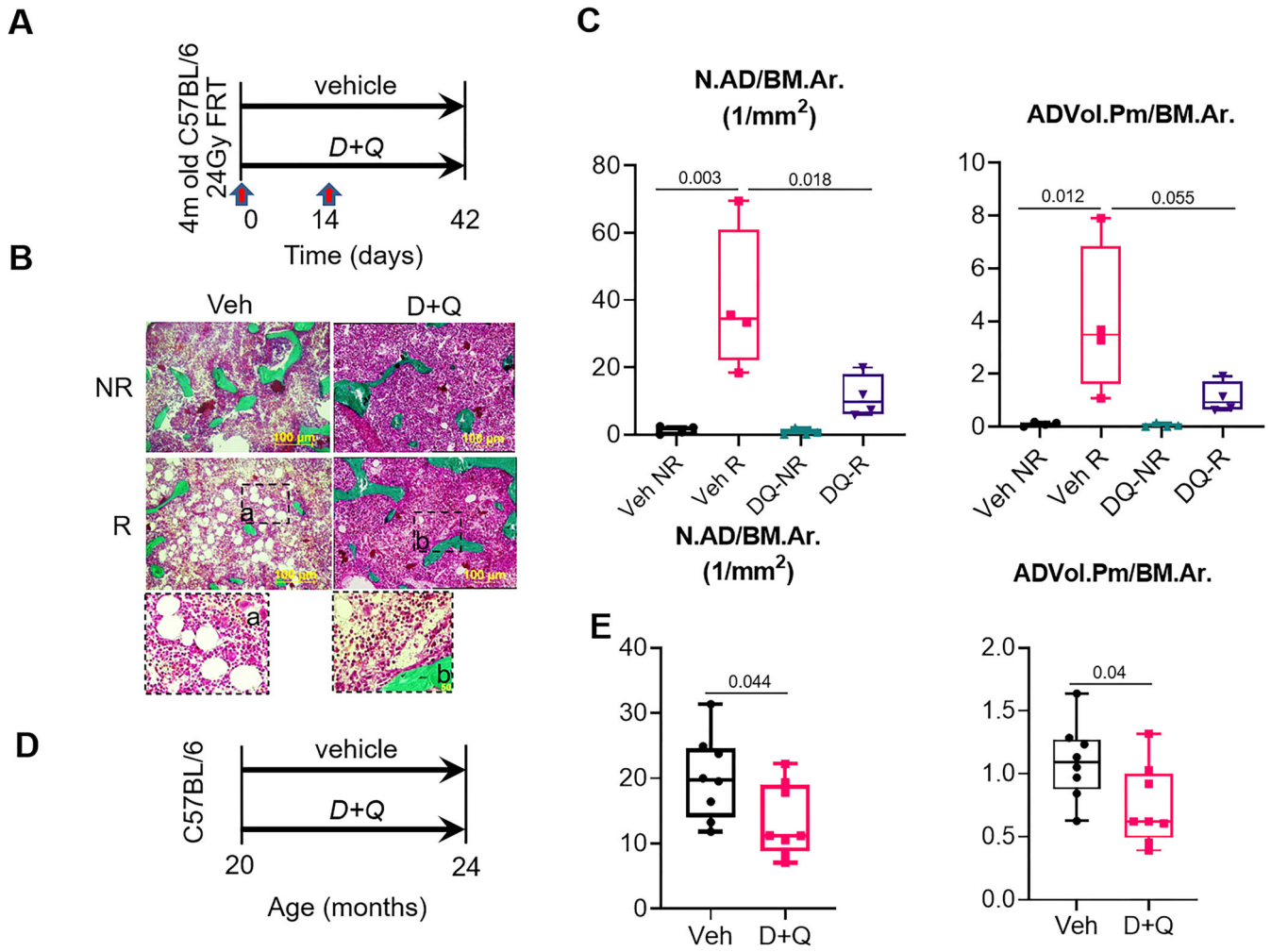

Fig. 6. Suppression of senescent cell burden ameliorates bone marrow adiposity in radiated and aged bone tissues. (*A*) A schematic representing the experimental design in which right femoral metaphyses of C57BL/6 mice were radiated (24 Gy) in a 5-mm region, while the equivalent region of the left leg served as control. Animals were treated with either vehicle ($n = 4$) or D + Q ($n = 4$) on days 0 and 14 postradiation and bones were analyzed histologically on day 42. (*B*) Representative images from plastic embedded 5-μm bone sections stained with Goldner's trichrome stain are shown. (*C*) Quantification of adipocyte number and adipocyte volume normalized against the BM.Ar. Data are shown as box-and-whisker plots (with median and interquartile range) from maximum to minimum, showing all data points. Statistical analyses were done using GraphPad Prism and *p* values were calculated using a two-way ANOVA ($\alpha = 0.05$) with Tukey's post hoc analysis. (*D*) Schematic representation of experimental design in which 20-month-old C57BL/6 received either vehicle or D + Q once a month for 4 months, and afterward the bones were processed for histomorphometry. (*E*) Adipocyte histomorphometric assessments are also presented for aged bones. Data are shown as box-and-whisker plots (with median and interquartile range) from maximum to minimum, showing all data points. Statistical analysis was performed using unpaired two-tailed *t* test. BM.Ar = bone marrow area.

Discussion

Bone is a metabolically active tissue with numerous cell types and a complex interplay of pathways that maintain an intricate balance of bone formation and resorption. Mesenchymal progenitors that generally contribute to bone formation also differentiate into marrow adipocytes, thereby causing a relative reduction in the osteoblast progenitor pool and disrupting bone homeostasis under conditions where adipogenesis is favored over osteogenesis. Increase in BMAT is a change observed across all instances of osteoporosis, is associated with reduced bone quality and fractures, and has been used as a predictor of osteoporosis.[4,27] Our previous studies support the idea that increased BMAT depletes the limited MSC pool and that MSCs undergo lineage switching toward an adipogenic cell fate in an aging microenvironment.[5,7] MSCs are known to be radioresistant.[28] Interestingly, it was recently shown that conditional deletion of Pparγ from early mesenchymal progenitors reduced BMAT but did not ameliorate thiazolidinedione-associated or age- associated bone loss, leading the authors to a conclusion that increasing BMAT does not contribute to age-associated bone loss.[29] Furthermore, targeted deletion of Pparγ in Dermo1-expressing mesenchymal lineage cells was shown to alleviate age-induced cortical bone loss in mice.[30] Overall, these studies suggest that BMAT seems to have a correlation with age-related bone loss; however, the trigger for BMAT during aging is still unknown.

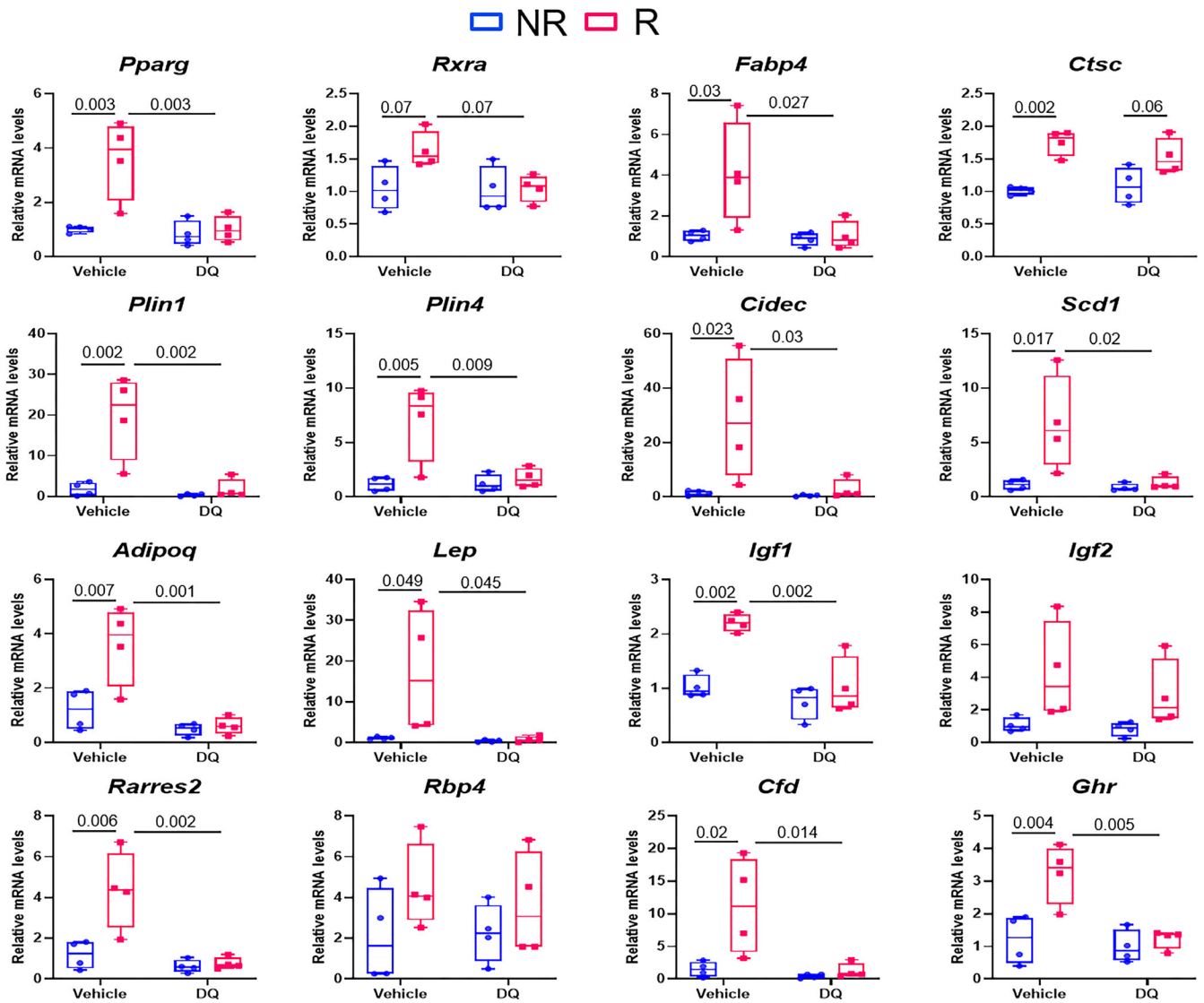

Fig. 7. Suppression of senescent cell burden decreases BMAT-related gene expression in radiated bones. Right femoral metaphyses of C57BL/6 mice were radiated (24 Gy) in a 5-mm region, while the equivalent region of the left leg served as control. Animals were treated with either vehicle ($n = 4$) or D + Q ($n = 4$) on days 0 and 14 postradiation and bones were harvested for mRNA. qRT-PCR was performed for 16 BMAT-related genes. Data are shown as box-and-whisker plots (with median and interquartile range) from maximum to minimum, showing all data points. Statistical analyses were done using GraphPad Prism and *p* values were calculated using a two-way ANOVA ($\alpha = 0.05$) with a Tukey's post hoc analysis.

In this study we identify cellular senescence as an important and early trigger of MSC cell fate switching toward adipogenesis during bone aging, using longitudinal assessments of senescence and BMAT-related genes in radiated bones (a model for clinical radiotherapy and accelerated bone aging), with parallel comparisons in aging bone. We have previously described the correlation between oxidative stress–induced DNA damage, a trigger for cellular senescence, and elevated levels of BMAT, as well as a reduction in BMAT with improved bone architecture.[5,14] Furthermore, we have previously showed that in telomere-based models of accelerated aging, BMAT was increased even in chronologically young animals.[31] Downregulation of WRN, a RecQ-type DNA helicase and DNA-repair protein, activates adipocyte-related genes in the preadipocyte cell line 3T3-L1.[32] Moreover, we have shown that an aged microenvironment influences the fate of young transplanted MSCs toward adiposity.[7] In this study our RNA-Seq data indicated that several BMAT-related genes were upregulated at 3 weeks postradiation. As shown in Table 1 several genes are associated with in vitro adipocyte differentiation, but not all are studied in the context of BMAT function in vivo. We showed a significant elevation of expression among these genes in R-bones as shown by RNA-Seq data (Fig. 1*A*) and confirmed the relevance of select few in an adipocyte differentiation assay in human MSCs (Fig. S2). A time course in radiated bones revealed that expression levels of these BMAT-related genes varied, but became more significant after 42 days, with 17 of the 20 tested showing significant upregulation. Plin1 staining in R-bones suggested that Plin1+ adipocytes were significantly elevated at day 7 postradiation, but nonexistent at day1 (Fig. 4*E*,*F*). This

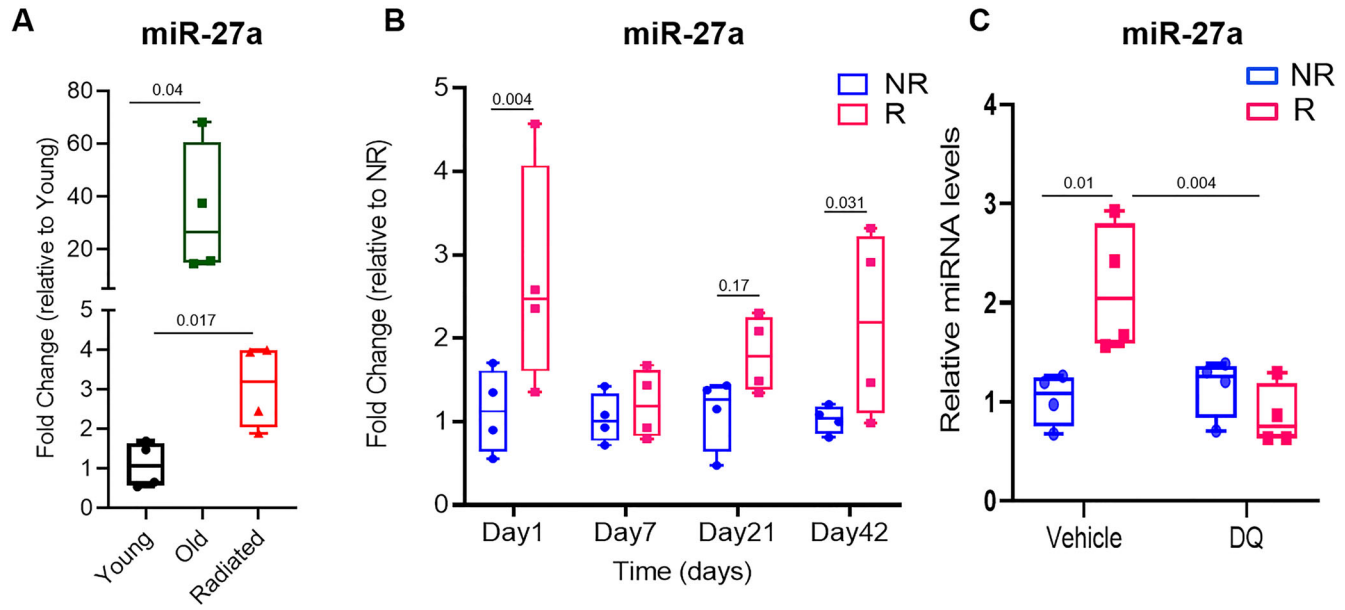

Fig. 8. Adiposity related microRNA 27a is positively correlated with senescence. Whole bones were collected from young (5 months old), old (24 months old), and radiated (5 months old) mice and mRNA was isolated. The cDNA was prepared using a miR reverse transcriptase kit and qRT-PCR was performed using primers for miR-27a (*A*). Statistical analyses were done using GraphPad Prism and *p* values were calculated using unpaired *t* test comparing young versus old and young versus radiated. (*B*) The right femoral metaphyses of C57BL/6 mice were radiated (24 Gy) in a 5-mm region, while the equivalent region of the left leg served as control. On days 1,7, 21, and 42 ($n = 4$ for each time point) R-femurs and NR-femurs were harvested for total mRNA isolation. The cDNA was prepared using a miR reverse transcriptase kit and qRT-PCR was performed using primers for miR-27a. Results are expressed as medians with interquartile range. Statistical analyses were done using GraphPad Prism and *p* values were calculated using a multiple *t* test. (*C*) Right femoral metaphyses of C57BL/6 mice were radiated (24 Gy) in a 5-mm region, while the equivalent region from the left leg served as control. Animals were treated with either vehicle ($n = 4$) or D + Q ($n = 4$) on days 0 and 14 postradiation and bones were harvested for mRNA on day 42. The cDNA was prepared using a miR reverse transcriptase kit and qRT-PCR was performed using primers for miR-27a. Data are shown as box-and-whisker plots (with median and interquartile range) from maximum to minimum, showing all data points. Statistical analyses were done using GraphPad Prism and *p* values were calculated using a two-way ANOVA ($\alpha = 0.05$) with a Tukey's post hoc analysis.

supported the gene expression data showing 11 of 20 BMAT genes being significantly upregulated at day 7 but not at day 1. Similarly, 18 of the tested 20 BMAT-related genes were markedly upregulated in 24-month-old bones. *Lepr* was one of the genes significantly expressed in the old but not R-bones, suggesting some slight underlying differences between aging and radiation effects. Histologically, R-bone and aged-bone look identical,[15] but this is the first evidence to our knowledge that shows an almost mirrored expression pattern in the BMAT-related genes between the two models. One of the points to consider while interpreting our data is the radiation dose. Although 24 Gy given focally induces changes similar to those found in aged bones, it is possible that lower doses of radiation may have a different effect on bone, depending on the extent and type of damage induced. However, low-dose radiation as low as 2 Gy has been shown to induce osteoclast activation and increase in BMAT, both features associated with aged bones. However, it remains to be studied whether these changes seen with low-dose radiation are also a senescence-driven process.

To understand the advent of aging-related changes to oxidative stress–related cellular senescence and BMAT, we used focal radiation as a surrogate, which allowed us to assess these changes longitudinally. Our data clearly show that senescence is established on day 1 in R-bones, shown by expression of *p21* mRNA using qRT-PCR (Fig. S3A), *p21* RNA-ISH in different cells of the BM compartment (Fig. 4*C*,*D*), and dysfunctional telomeres in osteocytes (Fig. 4*A*,*B*). It has been shown through in vitro experimentation that p21 is essential during adipocyte differentiation, where it not only induces cell cycle arrest but also maintains adipocyte hypertrophy.[33] Here we show that *p21* expression on day 1 precedes appearance of adipocytes on day 7 postradiation.[11,13] We also report here that the miRs that regulate *p21*, *miR-106b-5p*[24] and *miR-20a-5p*,[25] were both downregulated at different time points postradiation and with aging.

Genetic clearance of $p16^{Ink4a}$ senescent cells reduce age-related BMAT.[13] Reduction in the senescent cell burden by a senolytic cocktail of D + Q reduces both *p21* and $p16^{Ink4a}$ transcripts as well as the SASP.[11] Pharmacological treatment with the senolytic cocktail D + Q effectively clears senescent cells and suppresses the SASP in radiated[11] and aged[13] bones. Here we report that pharmacological treatment with D + Q significantly reduced radiation- and age-related adipocyte number and volume when normalized against the BM area. Even though BMAT-related genes correlate well with adipocyte numbers, we used our focal radiation model and confirmed the reduction in BMAT-related gene expression following senescent cell clearance by D + Q. p21/miR-106b/miR-20a regulation may drive cellular senescence in several bone marrow cells. As shown by Inoue and colleagues,[33] regulation of p21 may regulate adipocyte/BMAT related genes and thereby regulate MSC cell fate, which is also seen in R-bones. Because, by day 42, expression

levels of miR-106b or miR-20a in the R-bones returned to baseline levels seen in the controls, we could not assess the effects of D + Q on either of these miRNAs. Furthermore, suppression of the SASP by D + Q[11] reduces adipokine expression and potential secretion further regulating MSC cell fate. Because BMAT accumulation is inversely proportional to the MSC population and bone mineral density,[5] molecular regulation of BMAT could become a potential therapeutic option to treat age- and disease-related osteoporosis.

To identify an upstream molecular regulator of BMAT we studied *mir-27a-3p*, a miR that regulates *Pparg* and *Rxra*, expecting for this miR to decrease. Interestingly, we observed an increase in the levels of *miR-27a-3p* both in R-bones and aged-bones. However, this was consistent with several reports showing elevation of *miR-27a-3p* seen during adipocyte differentiation or in adipose tissue.[34] Because the primary target of *miR-27a-3p* is *Pparg* and *Rxra*, the increased levels of *miR-27a-3p* was thus an indicator of increased BMAT in which the miR-based downregulation of target genes occurs in synchrony. Hence, it is now understood that an elevated *miR-27a-3p* is a cellular negative feedback response to curb adipogenesis and counter *Pparg* or *Rxra*.[35] Interestingly, the senolytic cocktail of D + Q downregulated *miR-27a-3p*, and most of the radiation-induced BMAT genes, suggesting a direct correlation of senescent cells and elevation of BMAT. Interestingly, phosphodiesterase 3B (*Pde3B*), was the only BMAT-related gene (Fig. 1*B*, Table 1) that was predicted to be regulated by both miR-106b/mir-20a and mir-27a-3p (TargetScanMouse7.1) with binding sites in the 3′UTR of the *Pde3b* gene. Pde3b has been shown to be indispensable during the maintenance of the inflammatory nature of the adipose tissue,[36] and hence may play a role in the regulation of inflammatory cytokines including adipokines. Some of these cytokines that are part of the inflammasome may be traditional SASP factors, but some of them can be characterized as novel SASP factors.

Adipokines, the adipocyte-derived hormones, also referred to as inflammatory cytokines, secreted by the adipocytes, have detrimental effects on bone homeostasis. It is well understood now that adipokines and other secreted proteins from adipocytes interact with other cell types in the bone in a paracrine function, and potentially other organs of the body in a systemic manner.[37] Adipokines are known to potentiate the formation of new adipocytes and are often inflammatory in nature. Among the BMAT-related genes curated by us and expressed significantly in R-bones, we found several known adipokines, but some BMAT proteins previously not described as adipokines had a secretory signal sequence predicted by the Signal P software, suggesting that these proteins could be potential adipokines (Table 1).Chemerin is one such adipokine, which has been studied extensively. Early reports showed that the *Chemerin* (*Rarres2*) gene and its receptor gene *CMKLR1* (chemokine like receptor-1), were expressed in several organs[38] and cell types, including preadipocytes, macrophages, and mature adipocytes.[37] In our studies *Rarres2* expression increased in R-bones in a sequential manner, while being significantly expressed in the old-bones. Chemerin has been shown to induce osteoclastogenesis, and a neutralizing antibody against Chemerin blocks this process.[39] Some other adipokines such as Leptin (*Lep* gene), Adipsin (*Cfd* gene), Adiponectin (*Adipoq* gene), Visfatin (*Nampt* gene), and Vaspin (*Serpina12* gene) have been used as biomarkers that are inversely associated with bone health[40,41]; however, detailed mechanisms are still unknown. Although the *Nampt* gene was not detected in our RNA-Seq data, *Serpina12* was upregulated significantly (data not shown). In this study we show that the clearance of senescent cells could regulate adipokine expression in R-bones.

Based on the longitudinal studies in R-bones and pharmacological manipulation by D + Q, our data strongly suggests that senescence is the driving mechanism for MSC cell fate conversion to adiposity. Based on the gene expression profile of aged-bones and R-bones, our data also suggest that changes with radiation in an acute manner may represent an accelerated aging phenotype and may be used as a surrogate for physiological age-associated bone damage. Furthermore, although suppression of SASP factors as a group could regulate BMAT and maintain MSC cell fate, targeting individual adipokines may also regulate MSC cell fate and thus become a potential therapeutic to target age- and disease-related bone loss.

Acknowledgments

This work was made possible by the Eagle's Cancer Research Fund (to AC), Mayo Clinic Clinical and Translational Science Award (CTSA), grant number UL1TR002377, from the National Center for Advancing Translational Science (NCATS), a component of the National Institutes of Health (NIH) (to AC), and UL1TR000135, Center for Clinical and Translation Science (CCATS) (to DGM and AC), as well as the Robert and Arlene Kogod Professorship (to RJP); P01 AG062413 (to SK, JNF, and RJP), P01 AG004875 (to SK and DGM), R01 AG048792 (to SK and DGM), R01 AR068275 (to DGM), and R01 DK128552 (to JNF), and K01 AR070241 (to JNF). We thank Christine Hachfeld and Claire Wilhelm for their technical help with animal radiations.

Authors' roles: AC and RJP designed the study; AC, AL, JNF and MS performed the experiments; AC, DM, JNF, SK, JP, and RJP analyzed and interpreted the data. AC and RJP wrote the manuscript and all authors revised and approved the final version of the manuscript.

Author Contributions

Abhishek Chandra: Conceptualization; data curation; formal analysis; funding acquisition; investigation; methodology; project administration; resources; software; supervision; validation; visualization; writing – original draft; writing – review and editing. **Anthony B. Lagnado:** Data curation; investigation; methodology; validation; visualization; writing – review and editing. **Joshua Nicholas Farr:** Data curation; formal analysis; funding acquisition; investigation; methodology; writing – review and editing. **Megan Schleusner:** Data curation; formal analysis; methodology; writing – review and editing. **David G. Monroe:** Formal analysis; funding acquisition; investigation; software; validation; writing – review and editing. **Dominik Saul:** Data curation; formal analysis; software; validation; visualization; writing – review and editing. **Joao Passos:** Supervision; writing – review and editing. **Sundeep Khosla:** Formal analysis; funding acquisition; resources; writing – review and editing. **Robert Pignolo:** Conceptualization; project administration; resources; writing – original draft; writing – review and editing.

Conflict of Interest

The authors declare that the research was conducted in the absence of any commercial or financial relationships that could be construed as potential conflict of interest.

Peer Review

The peer review history for this article is available at https://publons.com/publon/10.1002/jbmr.4537.

Data Availability Statement

The data that support the findings of this study are available from the corresponding author upon reasonable request.

References

1. Chandra A, Rosenzweig A, Pignolo RJ. Osteobiology of Aging. In Pignolo RJ, Ahn J, eds. Fractures in the Elderly: A Guide to Practical Management. Cham: Springer International Publishing; 2018. pp. 3-37.
2. Veldhuis-Vlug AG, Rosen CJ. Clinical implications of bone marrow adiposity. J Intern Med. 2018;283:121-139.
3. Devlin MJ, Rosen CJ. The bone-fat interface: basic and clinical implications of marrow adiposity. Lancet Diabetes Endocrinol. 2015;3:141-147.
4. Woods GN, Ewing SK, Sigurdsson S, et al. Greater bone marrow adiposity predicts bone loss in older women. J Bone Miner Res. 2020;35:326-332.
5. Chandra A, Lin T, Young T, et al. Suppression of sclerostin alleviates radiation-induced bone loss by protecting bone-forming cells and their progenitors through distinct mechanisms. J Bone Miner Res. 2017;32:360-372.
6. Zhong L, Yao L, Tower RJ, et al. Single cell transcriptomics identifies a unique adipose lineage cell population that regulates bone marrow environment. Elife. 2020;9.
7. Singh L, Brennan TA, Russell E, et al. Aging alters bone-fat reciprocity by shifting in vivo mesenchymal precursor cell fate towards an adipogenic lineage. Bone. 2016;85:29-36.
8. Suchacki KJ, Cawthorn WP. Molecular interaction of bone marrow adipose tissue with energy metabolism. Curr Mol Biol Rep. 2018;4:41-49.
9. Hayflick L. The limited in vitro lifetime of human diploid cell strains. Exp Cell Res. 1965;37:614-636.
10. Coppe JP, Desprez PY, Krtolica A, Campisi J. The senescence-associated secretory phenotype: the dark side of tumor suppression. Annu Rev Pathol. 2010;5:99-118.
11. Chandra A, Lagnado AB, Farr JN, et al. Targeted reduction of senescent cell burden alleviates focal radiotherapy-related bone loss. J Bone Miner Res. 2020;35:1119-1131.
12. Farr JN, Fraser DG, Wang H, et al. Identification of senescent cells in the bone microenvironment. J Bone Miner Res. 2016;31:1920-1929.
13. Farr JN, Xu M, Weivoda MM, et al. Targeting cellular senescence prevents age-related bone loss in mice. Nat Med. 2017;23:1072-1079.
14. Chandra A, Wang L, Young T, et al. Proteasome inhibitor bortezomib is a novel therapeutic agent for focal radiation-induced osteoporosis. FASEB J. 2018;32:52-62.
15. Chandra A, Park SS, Pignolo RJ. Potential role of senescence in radiation-induced damage of the aged skeleton. Bone. 2019;120:423-431.
16. Kalari KR, Nair AA, Bhavsar JD, et al. MAP-RSeq: mayo analysis pipeline for RNA sequencing. BMC Bioinformatics. 2014;15:224.
17. Dobin A, Davis CA, Schlesinger F, et al. STAR: ultrafast universal RNA-seq aligner. Bioinformatics. 2013;29:15-21.
18. Liao Y, Smyth GK, Shi W. The Subread aligner: fast, accurate and scalable read mapping by seed-and-vote. Nucl Acids Res. 2013;41:e108.
19. McKenna A, Hanna M, Banks E, et al. The genome analysis toolkit: a MapReduce framework for analyzing next-generation DNA sequencing data. Genome Res. 2010;20:1297-1303.
20. Wang C, Davila JI, Baheti S, et al. RVboost: RNA-seq variants prioritization using a boosting method. Bioinformatics. 2014;30:3414-3416.
21. Wang L, Wang S, Li W. RSeQC: quality control of RNA-seq experiments. Bioinformatics. 2012;28:2184-2185.
22. Love MI, Huber W, Anders S. Moderated estimation of fold change and dispersion for RNA-seq data with DESeq2. Genome Biol. 2014;15:550.
23. Szklarczyk D, Gable AL, Nastou KC, et al. The STRING database in 2021: customizable protein-protein networks, and functional characterization of user-uploaded gene/measurement sets. Nucl Acids Res. 2021;49:D605-D612.
24. Ivanovska I, Ball AS, Diaz RL, et al. MicroRNAs in the miR-106b family regulate p21/CDKN1A and promote cell cycle progression. Mol Cell Biol. 2008;28:2167-2174.
25. Hackl M, Brunner S, Fortschegger K, et al. miR-17, miR-19b, miR-20a, and miR-106a are down-regulated in human aging. Aging Cell. 2010;9:291-296.
26. Lin Q, Gao Z, Alarcon RM, Ye J, Yun Z. A role of miR-27 in the regulation of adipogenesis. FEBS J. 2009;276:2348-2358.
27. Milisic L, Vegar-Zubovic S, Valjevac A. Bone marrow adiposity is inversely associated with bone mineral density in postmenopausal females. Med Glas (Zenica). 2020;17.
28. Nicolay NH, Lopez Perez R, Saffrich R, Huber PE. Radio-resistant mesenchymal stem cells: mechanisms of resistance and potential implications for the clinic. Oncotarget. 2015;6:19366-19380.
29. Almeida M, Kim HN, Han L, et al. Increased marrow adipogenesis does not contribute to age-dependent appendicular bone loss in female mice. Aging Cell. 2020;19:e13247.
30. Cao J, Ding K, Pan G, et al. Deletion of PPARgamma in mesenchymal lineage cells protects against aging-induced cortical bone loss in mice. J Gerontol A Biol Sci Med Sci. 2020;75:826-834.
31. Brennan TA, Egan KP, Lindborg CM, et al. Mouse models of telomere dysfunction phenocopy skeletal changes found in human age-related osteoporosis. Dis Model Mech. 2014;7:583-592.
32. Turaga RV, Paquet ER, Sild M, et al. The Werner syndrome protein affects the expression of genes involved in adipogenesis and inflammation in addition to cell cycle and DNA damage responses. Cell Cycle. 2009;8:2080-2092.
33. Inoue N, Yahagi N, Yamamoto T, et al. Cyclin-dependent kinase inhibitor, p21WAF1/CIP1, is involved in adipocyte differentiation and hypertrophy, linking to obesity, and insulin resistance. J Biol Chem. 2008;283:21220-21229.
34. Yu Y, Du H, Wei S, et al. Adipocyte-derived exosomal MiR-27a induces insulin resistance in skeletal muscle through repression of PPARgamma. Theranostics. 2018;8:2171-2188.
35. Deng K, Ren C, Fan Y, et al. miR-27a is an important adipogenesis regulator associated with differential lipid accumulation between intramuscular and subcutaneous adipose tissues of sheep. Domest Anim Endocrinol. 2020;71:106393.
36. Ahmad F, Chung YW, Tang Y, et al. Phosphodiesterase 3B (PDE3B) regulates NLRP3 inflammasome in adipose tissue. Sci Rep. 2016;6:28056.
37. MacDougald OA, Burant CF. The rapidly expanding family of adipokines. Cell Metab. 2007;6:159-161.
38. Bozaoglu K, Bolton K, McMillan J, et al. Chemerin is a novel adipokine associated with obesity and metabolic syndrome. Endocrinology. 2007;148:4687-4694.
39. Muruganandan S, Dranse HJ, Rourke JL, McMullen NM, Sinal CJ. Chemerin neutralization blocks hematopoietic stem cell osteoclastogenesis. Stem Cells. 2013;31:2172-2182.
40. Cervellati C, Bonaccorsi G, Bergamini CM, et al. Association between circulatory levels of adipokines and bone mineral density in postmenopausal women. Menopause. 2016;23:984-992.
41. Terzoudis S, Malliaraki N, Damilakis J, Dimitriadou DA, Zavos C, Koutroubakis IE. Chemerin, visfatin, and vaspin serum levels in relation to bone mineral density in patients with inflammatory bowel disease. Eur J Gastroenterol Hepatol. 2016;28:814-819.
42. Ambele MA, Dessels C, Durandt C, Pepper MS. Genome-wide analysis of gene expression during adipogenesis in human adipose-derived stromal cells reveals novel patterns of gene expression during adipocyte differentiation. Stem Cell Res. 2016;16:725-734.

43. Birsoy K, Berry R, Wang T, et al. Analysis of gene networks in white adipose tissue development reveals a role for ETS2 in adipogenesis. Development. 2011;138:4709-4719.

44. Kusuyama J, Komorizono A, Bandow K, Ohnishi T, Matsuguchi T. CXCL3 positively regulates adipogenic differentiation. J Lipid Res. 2016;57:1806-1820.

45. Secco B, Camire E, Briere MA, et al. Amplification of adipogenic commitment by VSTM2A. Cell Rep. 2017;18:93-106.

46. Kogame M, Matsuo S, Nakatani M, et al. ALK7 is a novel marker for adipocyte differentiation. J Med Invest. 2006;53:238-245.

47. Menssen A, Haupl T, Sittinger M, Delorme B, Charbord P, Ringe J. Differential gene expression profiling of human bone marrow-derived mesenchymal stem cells during adipogenic development. BMC Genomics. 2011;12:461.

48. Yin C, Xiao Y, Zhang W, et al. DNA microarray analysis of genes differentially expressed in adipocyte differentiation. J Biosci. 2014;39:415-423.

49. Ortega FJ, Vazquez-Martin A, Moreno-Navarrete JM, et al. Thyroid hormone responsive Spot 14 increases during differentiation of human adipocytes and its expression is down-regulated in obese subjects. Int J Obes (Lond). 2010;34:487-499.

50. Hotta K, Funahashi T, Matsukawa Y, et al. Galectin-12, an adipose-expressed galectin-like molecule possessing apoptosis-inducing activity. J Biol Chem. 2001;276:34089-34097.

51. Wang C, Li X, Dang H, et al. Insulin-like growth factor 2 regulates the proliferation and differentiation of rat adipose-derived stromal cells via IGF-1R and IR. Cytotherapy. 2019;21:619-630.

52. Scheideler M, Elabd C, Zaragosi LE, et al. Comparative transcriptomics of human multipotent stem cells during adipogenesis and osteoblastogenesis. BMC Genomics. 2008;9:340.

53. Goralski KB, McCarthy TC, Hanniman EA, et al. Chemerin, a novel adipokine that regulates adipogenesis and adipocyte metabolism. J Biol Chem. 2007;282:28175-28188.

54. Kobayashi S, Fukuhara A, Taguchi T, et al. Identification of a new secretory factor, CCDC3/Favine, in adipocytes and endothelial cells. Biochem Biophys Res Commun. 2010;392:29-35.

55. Ralston JC, Mutch DM. SCD1 inhibition during 3T3-L1 adipocyte differentiation remodels triacylglycerol, diacylglycerol and phospholipid fatty acid composition. Prostaglandins Leukot Essent Fatty Acids. 2015;98:29-37.

56. Bou M, Montfort J, Le Cam A, et al. Gene expression profile during proliferation and differentiation of rainbow trout adipocyte precursor cells. BMC Genomics. 2017;18:347.

57. Barneda D, Frontini A, Cinti S, Christian M. Dynamic changes in lipid droplet-associated proteins in the ''browning'' of white adipose tissues. Biochim Biophys Acta. 1831;2013:924-933.